The $pp \to p\Lambda K^+$ and $pp \to p\Sigma^0 K^+$ reactions with chiral dynamics

Ju-Jun Xie,[1,2,*] Hua-Xing Chen,[1,3,4,†] and E. Oset[1,3,‡]

[1]*Instituto de Física Corpuscular (IFIC), Centro Mixto CSIC-Universidad de Valencia, Institutos de Investigación de Paterna, Aptd. 22085, E-46071 Valencia, Spain*

[2]*Department of Physics, Zhengzhou University, Zhengzhou, Henan 450001, China*

[3]*Departamento de Física Teórica, Universidad de Valencia, Valencia, Spain*

[4]*Department of Physics and State Key Laboratory of Nuclear Physics and Technology, Peking University, Beijing 100871, China*

(Received 24 May 2011; revised manuscript received 19 July 2011; published 14 September 2011)

We report on a theoretical study of the $pp \to p\Lambda K^+$ and $pp \to p\Sigma^0 K^+$ reactions near threshold using a chiral dynamical approach. The production process is described by single-pion and single-kaon exchange. The final state interactions of nucleon-hyperon, K-hyperon, and K-nucleon systems are also taken into account. We show that our model leads to a fair description of the experimental data on the total cross section of the $pp \to p\Lambda K^+$ and $pp \to p\Sigma^0 K^+$ reactions. We find that the experimental observed strong suppression of Σ^0 production compared to Λ production at the same excess energy can be explained. However, ignorance of phases between some amplitudes does not allow one to properly account for the nucleon-hyperon final state interaction for the $pp \to p\Sigma^0 K^+$ reaction. We also demonstrate that the invariant mass distribution and the Dalitz plot provide direct information about the Λ and Σ^0 production mechanisms and may be tested by experiments at COSY or HIRFL-CSR.

DOI: 10.1103/PhysRevC.84.034004 PACS number(s): 13.30.Eg, 13.75.Cs, 14.20.Gk, 14.40.−n

I. INTRODUCTION

The $pp \to p\Lambda K^+$ and $pp \to p\Sigma^0 K^+$ reactions close to threshold have been advocated as a source of information on the $p\Lambda$ interaction due to a clear enhancement of the $p\Lambda$ invariant mass distribution close to threshold [1] with respect to a pure phase space expectation. The effect of the $p\Lambda$ final state interaction (FSI) has already been studied in Refs. [2,3], with a model for the $pp \to p\Lambda K^+$ and $pp \to p\Sigma^0 K^+$ based on π and K exchange and meson baryon amplitudes evaluated with the Juelich model. Further investigations have been carried out in Ref. [4] in terms of the inverse Jost function and the effective range approximation. More recently the issue of the FSI in these reactions has been reexamined in Refs. [5,6] using dispersion relations, and further experimental research has given more support to the role of the Λp FSI in these reactions [7]. A further investigation into the problem looked for angular distribution as a further observable that supported the importance of the Λp FSI [8]. With suitable parametrizations of the bare amplitude for the $pp \to p\Lambda K^+$ and $pp \to p\Sigma^0 K^+$ reactions prior to Λp FSI, a good reproduction of the shapes and ratio of the cross sections of the two reactions was obtained in a wide range of energies, considering FSI in the $pp \to p\Lambda K^+$ reaction but not in the $pp \to p\Sigma^0 K^+$ reaction. A different approach, with different results on the scattering lengths and effective range for the $p\Lambda$ interaction, is offered in Ref. [9].

Within a different approach to the problem, in Ref. [10] the authors give an explanation of the $pp \to pK^+\Lambda$ reaction based on the main mechanism of $N^*(1535)$ excitation mediated by π, η, and ρ exchange. Previous work on the issue included contributions from the excitation of the $N^*(1650)$, $N^*(1710)$, and $N^*(1720)$ resonances [11,12]. In Ref. [13] the authors show that the consideration of the FSI can make effects similar to the excitation of the $N^*(1535)$ resonance considered in Ref. [10], and the data of Ref. [14] support the excitation of the $N^*(1650)$ resonance. In a reply to Ref. [13], the authors of Refs. [15,16] argue that in the $J/\Psi \to \bar{p}K^+\Lambda$ reaction [17] the $N^*(1535)$ resonance is the most outstanding signal and they conclude that the inclusion of the $N^*(1535)$ resonance in the analysis of the $pp \to p\Lambda K^+$ reaction may reduce the $N^*(1650)$ contribution necessary to reproduce the data. In our approach, which relies upon pion and kaon exchange and chiral amplitudes, the $\pi N \to K\Lambda$ amplitude appears in the scheme, and the unitarization of this amplitude using the chiral unitary approach produces naturally the $N^*(1535)$ resonance [18–21], such that we can make a quantitative statement on its relevance in the $pp \to p\Lambda K^+$ reaction. On the other hand the $p\Lambda$ interaction close to threshold is very strong [22,23], and FSI due to this source is unavoidable in an accurate calculation and we also take it into account. We use a dynamical model similar to the one in Ref. [2] but we allow all pairs in the final state to undergo FSI, as a consequence of which we obtain a contribution from the $N^*(1535)$ resonance using chiral unitary amplitudes. Our approach also differs from the other approaches on how the FSI is implemented, and for this we follow the steps of Ref. [24]. In this reference the chiral unitary approach, where only scattering amplitudes are studied (asymptotic wave functions for $\vec{r} \to \infty$), is extended to obtain wave functions for all values of $\vec{r}$ and at the same time to determine form factors and effects of FSI in different reactions.

Furthermore, the experimental total cross section for the $pp \to p\Sigma^0 K^+$ reaction is strongly suppressed compared to that of the $pp \to p\Lambda K^+$ reaction at the same excess energy. This was explained by a destructive interference between π and

*xiejujun@ific.uv.es
†hxchen@ific.uv.es
‡oset@ific.uv.es

K exchange in the reaction $pp \to p\Sigma^0 K^+$ [2]. In Ref. [12], the Σ^0 strong suppression was reproduced by the inclusion of the contributions from $N^*(1650)$ resonances in the total cross sections of both $pp \to p\Lambda K^+$ and $pp \to p\Sigma^0 K^+$ reactions. We also find a reduction of the $pp \to p\Sigma^0 K^+$ cross section relative to that of $pp \to p\Lambda K^+$ at tree level and show that the nucleon-hyperon FSI can further magnify the difference.

In next section, we give the formalism and ingredients for our calculation. Then numerical results and discussion are given in Sec. III. Finally, a short summary is given in Sec. IV.

II. FORMALISM AND INGREDIENTS

To study the reactions $pp \to p\Lambda K^+$ and $pp \to p\Sigma^0 K^+$, first we investigate the possible reactions' mechanisms in this section. In the reaction at threshold, we consider the processes involving the exchange of π and K mesons as the dominant contributions, as in Ref. [2] and other works of the Juelich group. We show all the possible diagrams exchanging π and K mesons in Figs. 1 and 2, respectively. In the first diagram of Fig. 1, we show the definitions of the kinematics (p_1, p_2, p_3, p_4, p_5, and q) that we use in the present calculation.

The first diagrams of Figs. 1 and 2 show, respectively, the one π and K exchange, without further FSI. The rest of diagrams in Figs. 1 and 2 implement FSI from meson-baryon and baryon-baryon interactions of the final states. They are important when we work near the threshold and should be taken care of. We note that there are also the corresponding

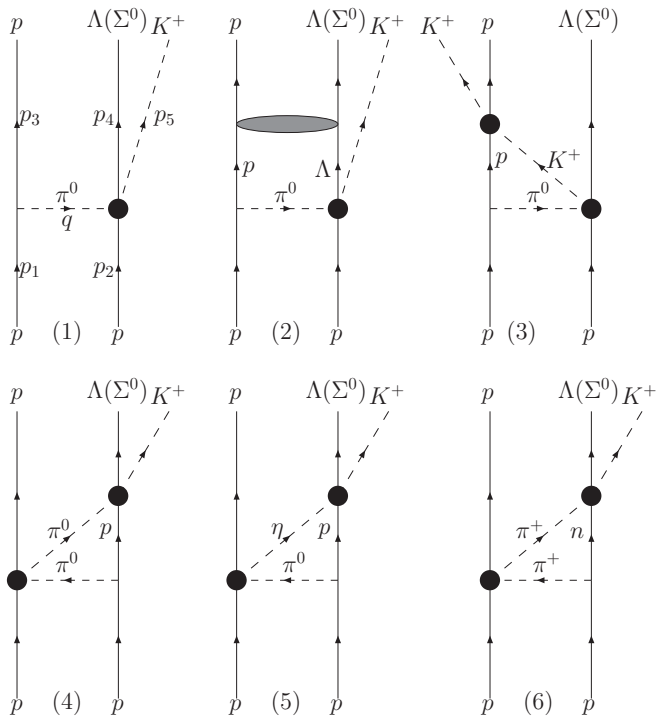

FIG. 1. The π-exchange mechanism of the $pp \to p\Lambda(\Sigma^0)K^+$ reactions. We have also included the FSIs. In the first diagram, we show the definitions of the kinematics (p_1, p_2, p_3, p_4, p_5, and q) that we use in the present calculation. In addition, we would have the analogous diagrams permuting the two baryons in the final states.

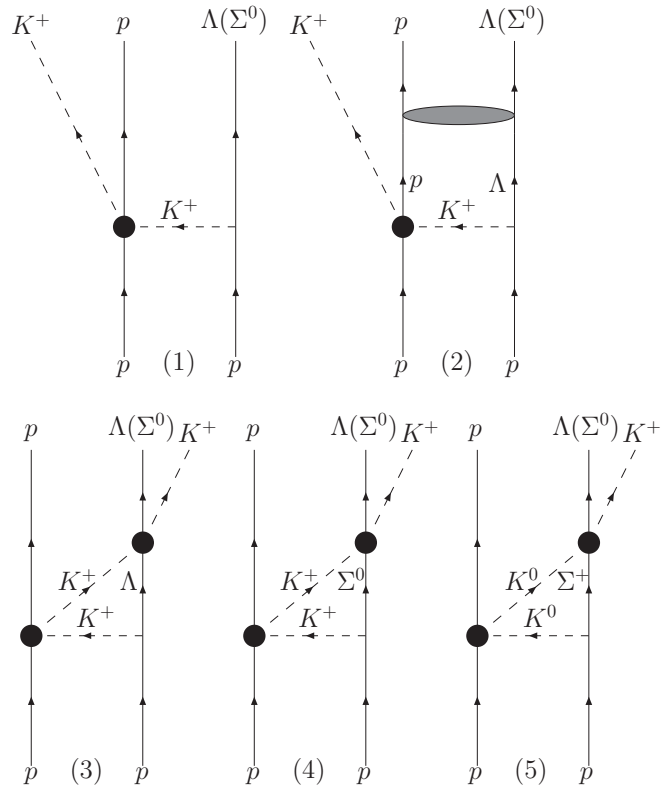

FIG. 2. The K-exchange mechanism of the $pp \to p\Lambda(\Sigma^0)K^+$ reactions.

"mirror" diagrams where the baryons p and $\Lambda(\Sigma^0)$ in the final states are permuted with each other. The final states of the two cases are orthogonal, although they contain the same particles; hence, there is no interference, but they contribute equally to the cross sections and this is taken into account.

Assuming an S wave for all the two-particle subsystems of the final states $p\Lambda(\Sigma^0)K^+$, which holds when we work near the reaction threshold, we can use the conservation of spin and parity symmetries and obtain that the initial proton-proton system, with isospin $I = 1$, has a total angular momentum $L = 1$ and a total spin $S = 1$; therefore, the spin wave functions for the initial proton-proton system are

$$|pp\rangle = \begin{cases} |1/2, 1/2\rangle|1/2, 1/2\rangle, \\ \frac{1}{\sqrt{2}}(|1/2, 1/2\rangle|1/2, -1/2\rangle + |1/2, -1/2\rangle|1/2, 1/2\rangle), \\ |1/2, -1/2\rangle|1/2, -1/2\rangle. \end{cases} \quad (1)$$

A. Elementary diagrams

To write out the total production amplitudes, first we try to write out the elementary production processes [the first diagrams labeled by (1) in Figs. 1 and 2]. There are two vertices. One of them is the strong vertex of πNN and KYN:

$$f_{\pi NN}\vec{\sigma}\cdot\vec{q}, \quad \text{and} \quad f_{KYN}\vec{\sigma}\cdot\vec{q}. \quad (2)$$

In this process we need several effective interactions for the strong πNN and KYN vertices as shown in the following:

$$f_{\pi^0 pp} = \frac{D+F}{2f_\pi}, \tag{3}$$

$$f_{\pi^+ pn} = \frac{D+F}{\sqrt{2}f_\pi}, \tag{4}$$

$$f_{K^+ p\Lambda} = \left(-\frac{D+F}{\sqrt{3}f_K} + \frac{D-F}{2\sqrt{3}f_K}\right), \tag{5}$$

$$f_{K^+ p\Sigma^0} = \frac{D-F}{2f_K}, \tag{6}$$

$$f_{K^0 p\Sigma^+} = \frac{D-F}{\sqrt{2}f_K}, \tag{7}$$

In the present work, we use the following parameter values: $f_\pi = 93$ MeV, $f_K = 1.22 f_\pi$ [25], $D = 0.795$, and $F = 0.465$ [26].

Another ingredient is the two-body meson-baryon scattering amplitudes such as $T_{\pi^0 p\to K^+\Lambda}$, etc. We use the chiral unitary theory to calculate them. The loop functions (G) and T matrices for a two-body meson-baryon system are well determined by a fit to the S_{11} and S_{31} partial wave of the πN scattering [20] and also the $\bar{K}N$ scattering [27]. Once these two-body amplitudes are fixed by the πN and $\bar{K}N$ scattering data, we can use them in the present calculation without introducing any new free parameter.

When we work in the center of mass coordinate of the initial states, we choose the momenta of the initial protons as $(0, 0, q_z)$ and $(0, 0, -q_z)$, and we can write the elementary diagrams for π and K exchange as [diagrams (1) of Figs. 1 and 2]

$$\mathcal{A}^1_\pi = -F_{\pi NN}(q^2) f_{\pi^0 pp}\sigma_z(1) q_z \frac{i}{q^2 - m_\pi^2} T_{\pi^0 p\to K^+\Lambda}, \tag{8}$$

$$\mathcal{A}^1_K = F_{KYN}(q^2) f_{K^+\Lambda p}\sigma_z(2) q_z \frac{i}{q^2 - m_K^2} T_{K^+ p\to K^+ p}, \tag{9}$$

where m_π and m_K are the masses of π and K mesons, $\sigma_z(1)$ and $\sigma_z(2)$ are the spin Pauli matrices acting on baryon 1 and baryon 2, and $F_{\pi NN}(q^2)$ and $F_{KYN}(q^2)$ are the form factors for the off-shell π and K mesons:

$$F_{\pi NN}(q^2) = \frac{\Lambda_\pi^2 - m_\pi^2}{\Lambda_\pi^2 - q^2}, \tag{10}$$

$$F_{KYN}(q^2) = \frac{\Lambda_K^2 - m_K^2}{\Lambda_K^2 - q^2}. \tag{11}$$

Here Λ_π and Λ_K are cutoff parameters where we take them equivalent in order to minimize the number of free parameters. This value is usually taken around 1 GeV in our calculations. We do a fine tuning of this value and obtain this value after comparing our theoretical results with the experimental data.

Similarly, we can obtain the "elementary production amplitudes" for the other diagrams. By this we mean the remnant of the diagram omitting the meson-baryon or baryon-baryon FSI. They are

$$\begin{aligned}
\mathcal{A}^2_\pi &= \mathcal{A}^3_\pi = \mathcal{A}^1_\pi, \\
\mathcal{A}^4_\pi &= F_{\pi NN}(q^2) f_{\pi^0 pp}\sigma_z(2) q_z \frac{i}{q^2 - m_\pi^2} T_{\pi^0 p\to\pi^0 p}, \\
\mathcal{A}^5_\pi &= F_{\pi NN}(q^2) f_{\pi^0 pp}\sigma_z(2) q_z \frac{i}{q^2 - m_\pi^2} T_{\pi^0 p\to\eta p}, \\
\mathcal{A}^6_\pi &= F_{\pi NN}(q^2) f_{\pi^+ pn}\sigma_z(2) q_z \frac{i}{q^2 - m_\pi^2} T_{\pi^+ p\to\pi^+ p}, \\
\mathcal{A}^2_K &= \mathcal{A}^3_K = \mathcal{A}^1_K, \\
\mathcal{A}^4_K &= F_{KYN}(q^2) f_{K^+\Sigma^0 p}\sigma_z(2) q_z \frac{i}{q^2 - m_K^2} T_{K^+ p\to K^+ p}, \\
\mathcal{A}^5_K &= F_{KYN}(q^2) f_{K^0\Sigma^+ p}\sigma_z(2) q_z \frac{i}{q^2 - m_K^2} T_{K^0 p\to K^0 p}.
\end{aligned} \tag{12}$$

B. Total amplitude and final state interactions

The total production amplitude $\mathcal{M}$ can be written in two parts:

$$\mathcal{M} = \mathcal{M}_\pi + \mathcal{M}_K, \tag{13}$$

where $\mathcal{M}_\pi$ and $\mathcal{M}_K$ are the amplitudes for those diagrams involving π and K exchange, respectively. We have the following formulas:

$$\mathcal{M}_\pi = \mathcal{A}^1_\pi + \sum_{i=2}^{6} \mathcal{A}^i_\pi G^i_\pi T^i_\pi, \tag{14}$$

$$\mathcal{M}_K = \mathcal{A}^1_K + \sum_{i=2}^{5} \mathcal{A}^i_K G^i_K T^i_K, \tag{15}$$

where $\mathcal{A}^i_{\pi/K}$ are the elementary production processes which we have obtained in Eqs. (8), (9), and (12). Together with the free two-body meson-baryon propagators (such as $G^3_\pi = G_{K^+p}$, etc.), baryon-baryon propagators (such as $G^2_\pi = G_{\Lambda p}$, etc.), and the FSIs for meson-baryon cases (such as $T^3_\pi = T_{K^+p\to K^+p}$, etc.) and for baryon-baryon cases ($T^2_\pi = T_{\Lambda p\to\Lambda p}$, etc.), we can easily write the full total production amplitude $\mathcal{M}$.

As we have discussed above, the meson-baryon G functions and T matrices have been calculated in previous references [20,27], and here we only need to deal with the baryon-baryon ones. Somewhat this is not an easy task from the theoretical point of view. However, we can obtain them using the experimental data. For this purpose we follow the strategy described below.

Following the factorized form of the T matrix [27,28], for the two-body Λp interaction we use the following type of $\Lambda p \to \Lambda p$ scattering amplitude:

$$T_{\Lambda p\to\Lambda p}(\sqrt{s_{p\Lambda}}) = \frac{1}{V^{-1} - G_{\Lambda p}(\sqrt{s_{p\Lambda}})}, \tag{16}$$

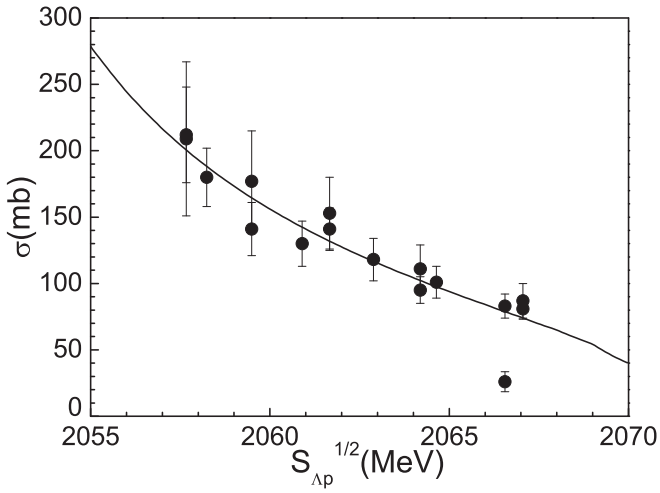

FIG. 3. Total cross sections vs the invariant mass $\sqrt{s_{p\Lambda}}$ for the $\Lambda p \to \Lambda p$ reaction. The experimental data are taken from Ref. [29].

where V is the Λp potential and $G_{\Lambda p}$ is the loop function for the Λp system,

$$G_{\Lambda p}(\sqrt{s_{p\Lambda}}) = i \int \frac{d^4q}{(2\pi)^4} \frac{M_\Lambda}{E_\Lambda(\mathbf{q})} \frac{1}{\sqrt{s_{p\Lambda}} - q^0 - E_\Lambda(\mathbf{q}) + i\epsilon} \times \frac{M_p}{E_p(\mathbf{q})} \frac{1}{q^0 - E_p(\mathbf{q}) + i\epsilon} = \int \frac{d^3q}{(2\pi)^3} \frac{M_\Lambda}{E_\Lambda(\mathbf{q})} \frac{M_p}{E_p(\mathbf{q})} \times \frac{1}{\sqrt{s_{p\Lambda}} - E_\Lambda(\mathbf{q}) - E_p(\mathbf{q}) + i\epsilon}, \quad (17)$$

which depends on the invariant mass $\sqrt{s_{p\Lambda}}$ of the $p\Lambda$ system and a cutoff parameter Λ.

Both V and Λ are determined using the experimental data of the $\Lambda p \to \Lambda p$ reaction. Here we assume that the potential V for near threshold $\Lambda p \to \Lambda p$ reaction is spin and energy independent since we find that this is good enough to explain the existent experiments. The $\Lambda p \to \Lambda p$ cross section is then assumed to be

$$\sigma_{\Lambda p \to \Lambda p} = \frac{M_p^2 M_\Lambda^2}{\pi s_{p\Lambda}} \left(\frac{3}{4} \left| T^{S=1}_{\Lambda p \to \Lambda p} \right|^2 + \frac{1}{4} \left| T^{S=0}_{\Lambda p \to \Lambda p} \right|^2 \right), \quad (18)$$

with $T^{S=1} = T^{S=0}$ in our assumption.

Then, by comparing the theoretical total cross sections of $\Lambda p \to \Lambda p$ reaction with experimental data, we can extract the value of the potential V and the cutoff Λ (as shown in Fig. 3):

$$V = -6.0 \times 10^{-5}\,\mathrm{MeV}^{-2}, \quad \text{and} \quad \Lambda = 130\,\mathrm{MeV}. \quad (19)$$

On the other side, the scattering amplitude $T_{\Lambda p \to \Lambda p}(\sqrt{s_{p\Lambda}})$ can be also expressed by using the effective range approximation in the field theory as

$$T_{\Lambda p \to \Lambda p}(\sqrt{s_{p\Lambda}}) = \frac{2\pi \sqrt{s_{p\Lambda}}}{M_p M_\Lambda} \frac{1}{\frac{1}{\bar{a}} - \frac{1}{2}\bar{r}k^2 + ik}, \quad (20)$$

where k is the momentum of the Λ or the p in the Λp center of mass frame, which is given by

$$k = \frac{\sqrt{[s_{p\Lambda} - (M_\Lambda + M_p)][s_{p\Lambda} - (M_\Lambda - M_p)^2]}}{2\sqrt{s_{p\Lambda}}}. \quad (21)$$

By comparing Eq. (20) with Eq. (16), we can easily get

$$\frac{M_\Lambda M_p}{2\pi \sqrt{s_{p\Lambda}}} \left(\frac{1}{\bar{a}} - \frac{1}{2}\bar{r}k^2 \right) = V^{-1} - \mathrm{Re}[G_{\Lambda p}(\sqrt{s_{\Lambda p}})], \quad (22)$$

$$\frac{M_\Lambda M_p}{2\pi \sqrt{s_{p\Lambda}}} k = -\mathrm{Im}[G_{\Lambda p}(\sqrt{s_{\Lambda p}})], \quad (23)$$

with $\mathrm{Re}[G_{\Lambda p}(\sqrt{s_{\Lambda p}})]$ and $\mathrm{Im}[G_{\Lambda p}(\sqrt{s_{\Lambda p}})]$ being the real and imaginary parts of $G_{\Lambda p}(\sqrt{s_{\Lambda p}})$, respectively. From Eq. (22), we can get the scattering length $\bar{a} = (-1.75 \pm 0.02)$ fm and effective range $\bar{r} = (3.43 \pm 0.07)$ fm by using the values of $V = -6.0 \times 10^{-5}$ MeV^{-2} and $\Lambda = 130$ MeV. Equation (23) follows exactly because it expresses unitarity, and the amplitude of Eq. (16) together with Eq. (17) satisfies unitarity. The value of Λ is relatively small, but this is typical for baryon-baryon interactions reflecting the long range of one- or two-pion exchange. One should not use this cutoff methods if Λ is smaller than the baryons' momentum in the scattering, but this is not the case in the range of Fig. 3 or the range needed in the FSI in Figs. 1(2) and 2(2) for the experiments of Refs. [30,31].

C. The transition between $pp \to p\Lambda K^+$ and $pp \to p\Sigma^0 K^+$

Without considering the transition between $p\Lambda$ and $p\Sigma^0$, we can obtain the amplitudes of $pp \to p\Lambda K^+$ and $pp \to p\Sigma^0 K^+$. The results are shown in the following section where we find that the first one is much larger than the second one. Therefore, for $pp \to p\Lambda K^+$ we do not need to consider $pp \to p\Sigma^0 K^+ \to p\Lambda K^+$, but for $pp \to p\Sigma^0 K^+$ we have to consider $pp \to p\Lambda K^+ \to p\Sigma^0 K^+$ (We shall be more quantitative below).

After considering the $p\Lambda \to p\Sigma^0$ transition diagrams [Fig. 1(2) and Fig. 2(2)], the scattering amplitude of the $pp \to p\Sigma^0 K^+$ reaction can be rewritten as two parts with a relative phase ϕ,

$$\mathcal{M} = \mathcal{M}_1 + e^{i\phi}\mathcal{M}_2, \quad (24)$$

where $\mathcal{M}_1$ is the basic amplitude without including the transition process, and $\mathcal{M}_2$ is the transition amplitude:

$$\mathcal{M}_2 = \mathcal{M}_{pp \to p\Lambda K^+} G_{\Lambda p} T_{\Lambda p \to \Sigma^0 p}. \quad (25)$$

Here we note that the reaction threshold of Σ^0 production is much higher than the Λ production, and hence we cannot calculate $\mathcal{M}_{pp \to p\Lambda K^+}$ using our previous result. Again we use the experimental data of the high-energy $pp \to p\Lambda K^+$ reaction [32]. Under a pure phase space expectation we find that a constant value $\mathcal{M}_{pp \to p\Lambda K^+} = 1.37 \times 10^{-7}$ MeV^{-3} is

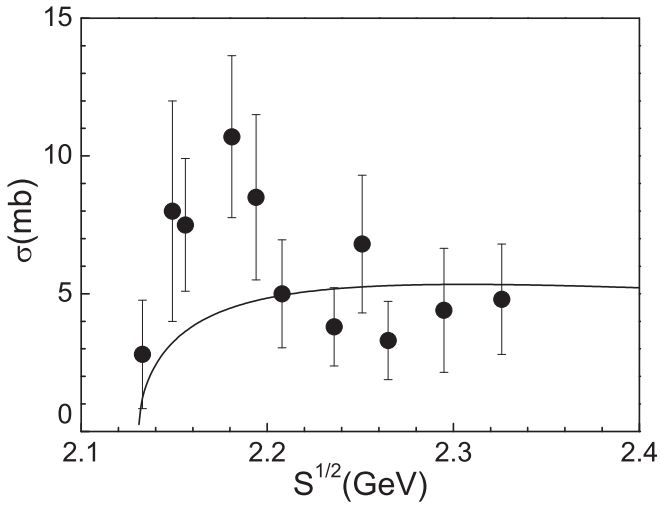

FIG. 4. Cross sections of the $\Lambda p \to \Sigma^0 p$ reaction. The experimental data are taken from Ref. [33].

consistent with the experimental data. Similarly, the transition amplitude $T_{\Lambda p\to\Sigma^0 p}$ is also taken as a constant. Compared with the experimental data of the $\Lambda p \to \Sigma^0 p$ scattering

$$\sigma_{\Lambda p\to\Sigma^0 p} = \frac{M_p^2 M_{\Sigma^0}^2}{\pi s_{p\Lambda}} \frac{p_{\Sigma^0}^{\text{c.m.}}}{p_{\Lambda}^{\text{c.m.}}} |T_{\Lambda p\to\Sigma^0 p}|^2, \tag{26}$$

we can get this constant $T_{\Lambda p\to\Sigma^0 p} = 1.53 \times 10^{-5}$ MeV^{-2}. We show our theoretical results for the $\Lambda p \to \Sigma^0 p$ cross section in Fig. 4 by the solid line. Although the agreement is not perfect, it is sufficient for the qualitative study that we do in the present study of the FSI in the $pp \to p\Sigma^0 K^+$ reaction.

It is worth noting that from the total cross section of $pp \to p\Lambda K^+$ and $\Lambda p \to \Sigma^0 p$ reactions we can only get the moduli of $\mathcal{M}_{pp\to p\Lambda K^+}$ and $T_{\Lambda p\to\Sigma^0 p}$. However, because we need to put a relative phase ϕ between $\mathcal{M}_1$ and $\mathcal{M}_2$ in Eq. (24), the phase of $\mathcal{M}_{pp\to p\Lambda K^+}$ and $T_{\Lambda p\to\Sigma^0 p}$ can be absorbed into the parameter ϕ, which is introduced in Eq. (24). So, in Eq. (25), we only need to use the modules for $\mathcal{M}_{pp\to p\Lambda K^+}$ and $T_{\Lambda p\to\Sigma^0 p}$.

The $G_{\Lambda p}$ function in Eq. (25) should not be the same as that for Λp scattering of lower energies because the Λp energy in this case is higher. We can already see the first problem that we face to get a quantitative description of the nucleon-hyperon FSI in this case. Here we adopt a phenomenological approach fitting the relative phase ϕ and the cutoff parameter Λ of $G_{\Lambda p}$ trying to reproduce the $pp \to p\Sigma^0 K^+$ cross section, keeping in mind that Λ should be of the same order of magnitude as for lower energies, but not necessarily equal. As a consequence, we do not claim a precise prediction of this cross section.

D. Total cross section

From Eqs. (13) and (24) we can easily get the invariant amplitude square $|\mathcal{M}|^2$, then the calculation of the total cross section $\sigma(pp \to p\Lambda(\Sigma^0)K^+)$ is straightforward:

$$d\sigma[pp \to p\Lambda(\Sigma^0)K^+] = \frac{1}{3}\frac{M_p^2}{F}\sum_{\text{spins}}|\mathcal{M}|^2 \times \frac{M_p d^3 p_p}{E_p}\frac{M_{\Lambda(\Sigma^0)} d^3 p_{\Lambda(\Sigma^0)}}{E_{\Lambda(\Sigma^0)}} \times \frac{d^3 p_{K^+}}{2E_{K^+}}\delta^4(p_1 + p_2 - p_3 - p_4 - p_5), \tag{27}$$

where the flux factor is

$$F = (2\pi)^5\sqrt{(p_1 \cdot p_2)^2 - M_p^4}. \tag{28}$$

Here we want to discuss a bit about the effect of the spin factor σ_z of Eqs. (8), (9), and (12). For $S_{\Lambda p} = 1$, the initial and final spin structures are both symmetric, and so the σ_z acting on the first proton and second proton would lead to the same result. For $S_{\Lambda p} = 0$, the initial spin structure is symmetric and the final is antisymmetric, and so the σ_z acting on the first proton and second proton would lead to the different result: it gives an extra minus sign when acting on the second proton.

Now we address the question of the contribution to the $pp \to p\Lambda K^+$ reaction from the transition of the $pp \to p\Sigma^0 K^+ \to p\Lambda K^+$ process. By analogy Eq. (25) is given by

$$\mathcal{M}_2' = \mathcal{M}_{pp\to p\Sigma^0 K^+} G_{\Sigma^0 p} T_{\Sigma^0 p\to\Lambda p}. \tag{29}$$

Then the relative contribution to the main $pp \to p\Lambda K^+$ term is

$$R_\Lambda = \frac{\mathcal{M}'_2}{\mathcal{M}'_1}, \tag{30}$$

where $\mathcal{M}'_1$ is the main $pp \to p\Lambda K^+$ amplitude without considering the $p\Sigma^0 \to p\Lambda$ transition.

Similarly, the relative contribution of $\mathcal{M}_2$ of Eq. (25) to $\mathcal{M}_1$ of Eq. (24) for the $pp \to p\Sigma^0 K^+$ reaction is given by

$$R_\Sigma = \frac{\mathcal{M}_2}{\mathcal{M}_1}. \tag{31}$$

Hence the ratio of the two ratios is

$$\frac{R_\Lambda}{R_\Sigma} = \frac{\mathcal{M}'_2}{\mathcal{M}'_1}\frac{\mathcal{M}_1}{\mathcal{M}_2} = \frac{(\mathcal{M}_{pp\to p\Sigma^0 K^+})^2}{(\mathcal{M}_{pp\to p\Lambda K^+})^2}\frac{G_{\Sigma^0 p}}{G_{\Lambda p}}. \tag{32}$$

The ratio of the amplitudes squared is of the order of the ratio of the cross sections of the respective reactions for a same excess energy and $|G_{\Sigma^0 p}|$ is smaller than $|G_{\Lambda p}|$ at the threshold of Λp (by a factor of about 3.5). As a consequence, the contribution of the transition $pp \to p\Sigma^0 K^+ \to p\Lambda K^+$ relative to the main $pp \to p\Lambda K^+$ amplitude is about 100 times smaller than the contribution of the $pp \to p\Lambda K^+ \to p\Sigma^0 K^+$ transition relative to the main $pp \to p\Sigma^0 K^+$ amplitude and can be neglected.

III. NUMERICAL RESULTS AND DISCUSSION

With the formalism and ingredients given above, the total cross section versus the excess energy (ε) for the $pp \to p\Lambda K^+$ and $pp \to p\Sigma^0 K^+$ reactions is calculated by using a Monte Carlo multiparticle phase space integration program. The

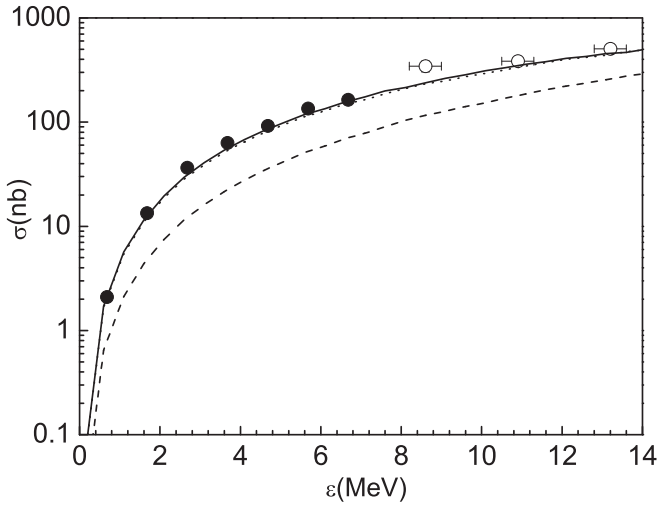

FIG. 5. Total cross section vs excess energy ε for the $pp \to p\Lambda K^+$ reaction compared with experimental data from Refs. [30] (solid circles) and [31] (open circles). Solid and dashed lines show the results from our model with and without including the $p\Lambda$ FSI, respectively, while the dotted line represents the results by using the $p\Lambda$ FSI parameters from Ref. [9].

results for ε from 0 to 14 MeV are shown in Figs. 5 and 6 with the cutoff $\Lambda_\pi = \Lambda_K = 1300$ MeV, together with the experimental data [30,31] for comparison.

A. The $pp \to p\Lambda K^+$ cross section

In Fig. 5, we show our results for the case of the $pp \to p\Lambda K^+$ reaction. The solid and dashed lines show the results from our model with and without including the $p\Lambda$ FSI [depicted by Figs. 1(2) and 2(2)], respectively. Alternatively, we also perform another calculation by using the effective range approximation for the $T_{\Lambda p\to\Lambda p}$ in the FSI with the parameters taken from Ref. [9] ($a_s = -2.43$ fm and $r_s = 2.21$ fm for the spin of Λp system $S_{\Lambda p} = 0$; $a_t = -1.56$ fm and $r_t = 3.7$ fm for $S_{\Lambda p} = 1$). The results are shown in Fig. 5 using the dotted line. The spin structure of the amplitudes is such that one has a weight twice bigger for the transition to $S_{\Lambda p} = 1$ than to $S_{\Lambda p} = 0$. Thus, this fact is implemented by changing $T_{\Lambda p\to\Lambda p}$ of Eq. (16) by that of Eq. (20) with the a_i and r_i parameters while using the same $G_{\Lambda p}$ loop function. The weighted cross section $\frac{1}{3}(2\sigma_{S=1} + \sigma_{S=0})$ is taken.

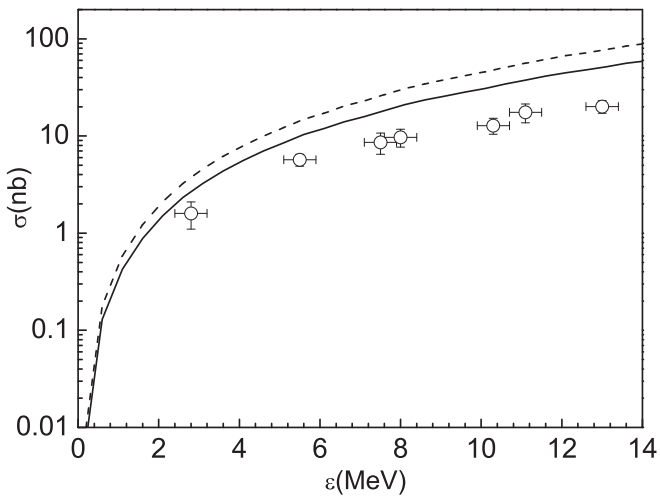

FIG. 6. Total cross section vs excess energy ε for the $pp \to p\Sigma^0 K^+$ reaction compared with experimental data from Ref. [31]. Solid and dashed lines show the results from our model with and without including the $p\Lambda \to p\Sigma^0$ transition diagram, respectively.

We can see that in Fig. 5 both the solid and dotted lines, which were obtained by including the $p\Lambda$ FSI with different methods, can reproduce the experimental data quite well for the excess energy ε lower than 14 MeV, but the dashed line is about 2.5 times smaller than the experimental data at threshold but less than a factor of 2 smaller than experimental data at $\epsilon \sim 14$ MeV. This indicates that the $p\Lambda$ FSI is very important in the $pp \to p\Lambda K^+$ reaction close to threshold. This energy dependence of the FSI is what allows the determination of the ΛN interaction in other approaches that do not try to get absolute cross sections [9,34].

It is interesting to note that the spin-averaged parameters $\bar{a}$ and $\bar{r}$ deduced from our approach are very similar to those of the triplet parameters a_t and r_t in Ref. [9] (which have largest weight in the cross sections), obtained from the best fit of both the missing mass spectrum of the reaction $pp \to K^+ + (p\Lambda)$ and the free Λp scattering by using the standard Jost function approach. Moreover, our results show that only two parameters in the $p\Lambda$ interaction are enough to reproduce the current lower energy experimental data on the $\Lambda p \to \Lambda p$ and $pp \to p\Lambda K^+$ reactions, but equally good results could be obtained with the parameters of Ref. [9]. This indicates that one should accept the differences between the results in our approach and those of Ref. [9] as uncertainties in the determination of these parameters.

B. The $pp \to p\Sigma^0 K^+$ cross section

For the case of the $pp \to p\Sigma^0 K^+$ reaction we need minor changes with respect to the $pp \to p\Lambda K^+$ reaction. In A_π^1 and A_K^1 we replace Λ by Σ^0 in the final states. In the other rescattering diagrams evaluated in Eqs. (14) and (15) we replace T_π^i and T_K^i by substituting Λ by Σ^0 in the final states. This takes into account the $\Lambda p \to \Sigma^0 p$ transition, which we argued before was an important term to consider.

In Fig. 6, our results for $pp \to p\Sigma^0 K^+$ reaction are shown. The solid and dashed lines show the results from our model with and without including the $p\Lambda \to p\Sigma^0$ transition diagrams, respectively. The solid line is obtained using $\Lambda = 310$ MeV and a relative phase $\phi = \pi/2$ between the basic $pp \to p\Sigma^0 K^+$ amplitude ($\mathcal{M}_1$) and the transition $pp \to (p\Lambda)K^+ \to (p\Sigma^0)K^+$ amplitude ($\mathcal{M}_2$). We can see that the FSI mechanism that we have discussed can indeed induce a reduction of the $pp \to p\Sigma^0 K^+$ reaction, but we mentioned that we do not have control over Λ and ϕ. On the other hand, we should mention at this point that the mechanism of $pp \to p\Sigma^0 K^+$ production with $p\Sigma^0$ FSI, which we have not considered, should be equally relevant. Indeed, counting simply cross sections we have at

4 MeV energy excess $\sigma_{pp\to p\Lambda K^+}\sigma_{p\Lambda\to p\Sigma^0} \sim 70\,\text{mb} \times 5\,\text{mb}$ while $\sigma_{pp\to p\Sigma^0 K^+}\sigma_{p\Sigma^0\to p\Sigma^0} \sim 7\,\text{mb} \times 90\,\text{mb}$, which indicates that the strength of the two amplitudes introduced in the nucleon-hyperon FSI is similar. The FSI in this case involves two coupled channels in which we do not have control of interferences. This means that we do not have at hand enough information within the present formalism to properly face the nucleon-hyperon FSI in this case. This stated, the exercise done indicates that this FSI could account for the difference of our results without this FSI and the data. On the other hand, we also found that the strong reduction of the $pp \to p\Sigma^0 K^+$ cross section with respect to the $pp \to p\Lambda K^+$ one is described by our model at a semiquantitative level.

C. Invariant mass spectra and Dalitz plot

In Figs. 7 and 8, we give our prediction for the invariant mass spectra and the Dalitz plot for $pp \to p\Lambda K^+$ and $pp \to p\Sigma^0 K^+$ reactions at excess energy $\varepsilon = 13$ MeV. The dashed line reflects the pure phase space, while the solid lines include the full amplitudes. The $p\Lambda$ FSI is very strong and can be seen in the invariant mass distribution of the $p\Lambda$ system in Fig. 7.

In Fig. 7, the invariant mass distribution of $K^+\Lambda$ is interesting and counterintuitive. Indeed, we have introduced explicitly the FSI of the $K^+\Lambda$ state, which is dominated by the $N^*(1535)$ resonance below threshold in our approach. We should expect that the solid line, accounting for the FSI should be shifted to lower invariant masses as a consequence of the presence of the $N^*(1535)$ resonance below threshold. However the opposite effect is observed. This is a consequence of the strong effect of the Λp FSI and we have observed that

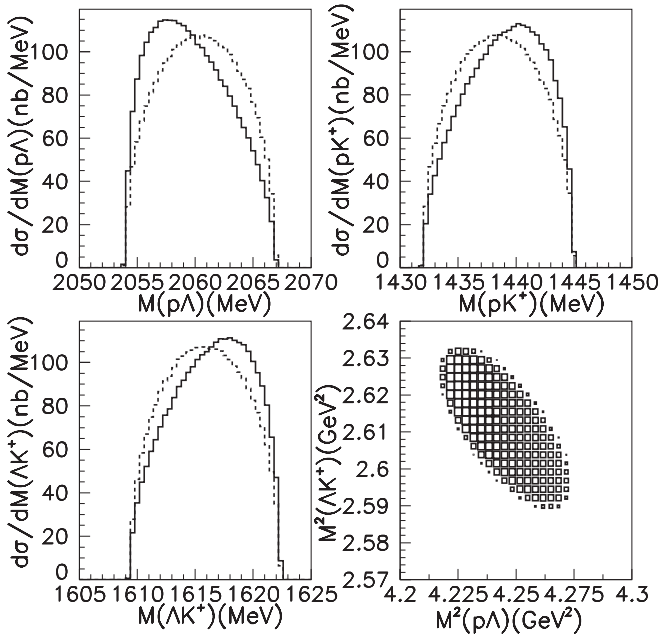

FIG. 7. The invariant mass spectra and the Dalitz plot for the $pp \to p\Lambda K^+$ reaction at excess energy $\varepsilon = 13$ MeV with the contributions from the full amplitude (solid curve), compared with pure phase space distributions (dashed curve).

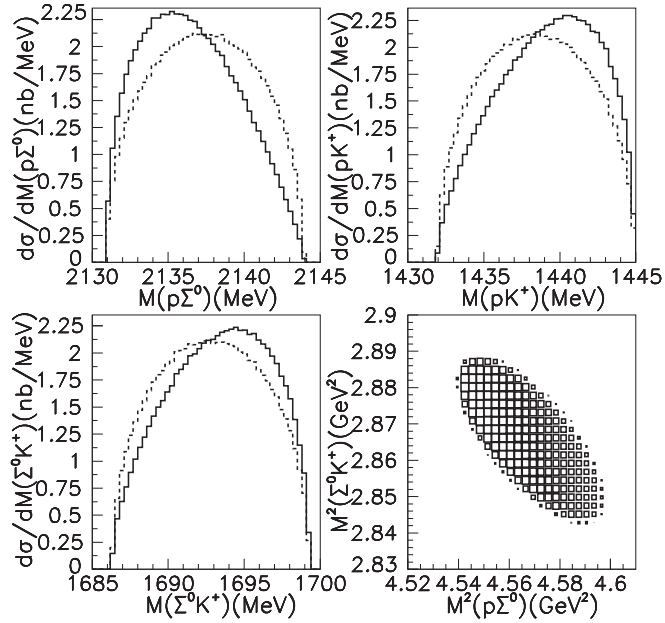

FIG. 8. The invariant mass spectra and the Dalitz plot for the $pp \to p\Sigma^0 K^+$ reaction at excess energy $\varepsilon = 13$ MeV with the contributions from the full amplitude (solid curve), compared with pure phase space distributions (dashed curve).

by removing this Λp FSI the solid line in the $K^+\Lambda$ mass distribution is indeed shifted to lower invariant mass with respect to phase space.

In Fig. 8 we have taken the nucleon-hyperon FSI from the $p\Lambda \to p\Sigma^0$ transition discussed in the text. We can see features from the FSI in the invariant mass distribution that can help us understand these effects better by comparison with future experiments.

The invariant mass spectra and the Dalitz plots in Figs. 7 and 8 are direct information about the Λ and Σ^0 production mechanism and may be tested by experiments at COSY or HIRFL-CSR.

IV. SUMMARY

We have made a theoretical study of the $pp \to p\Lambda K^+$ and $pp \to p\Sigma^0 K^+$ reactions involving π and K exchange and implementing FSIs of any of the two hadron pairs in the final states. The amplitudes and loop functions involved have been obtained using the chiral unitary approach for meson-baryon interactions [20,27]. The aims were two. First we wanted to see if the theory provides a fair description of the cross sections for these two reactions, including the factor around 30 smaller cross sections of the $pp \to p\Sigma^0 K^+$ reaction than for the $pp \to p\Lambda K^+$ one at similar excess energies. We found that the theory indeed accomplished that qualitatively.

Second, we wanted to see the effect of the FSI and eventually determine the $\Lambda p \to \Lambda p$ low-energy parameters, scattering length, and effective range. Here we also succeeded and found reasonable parameters compatible with the low-energy $\Lambda p \to \Lambda p$ transition cross section and the

$pp \to p\Lambda K^+$ cross section. These results are also compatible with those determined in a recent empirical analysis [9], but we were able to show that there are intrinsic uncertainties in the determination of these parameters from these data, in particular the separation of the results for the $S = 1$ and $S = 0$ Λp systems. For the case of the $pp \to p\Sigma^0 K^+$ reaction, with much smaller cross sections than the $pp \to p\Lambda K^+$ reaction, we could obtain qualitative results, but the FSI was influenced by the $\Lambda p \to \Sigma^0 p$ transition which required extra information than the one deduced and used in the $pp \to p\Lambda K^+$ reaction close to threshold. In this case we have implemented the FSI by introducing a couple of parameters (a phase and a cutoff) to the data, within a reasonable range. A better agreement with experiment could be found, but certainly one does not obtain a quantitative theoretical prediction. We also show that one should also consider the nucleon-hyperon FSI from the $p\Sigma^0 \to p\Sigma^0$ amplitude, but one would not know the interference between the two mechanisms. The results obtained for a and r for the ΛN interaction at low energies are valuable as empirical determinations of these data, in line with other determinations. However, by using realistic amplitudes extracted from the chiral unitary approach, we could also show that a determination of the absolute value of the cross sections is possible, in line with similar findings with amplitudes from the Juelich model.

We also made predictions for the invariant mass distributions and Dalitz plots that can be used for comparison with future experiments.

ACKNOWLEDGMENTS

This work is partly supported by DGICYT Contracts No. FIS2006-03438 and No. FPA2007-62777, the Generalitat Valenciana in the program PROMETEO, and the EU Integrated Infrastructure Initiative Hadron Physics Project under Grant No. 227431. Ju-Jun Xie acknowledges Ministerio de Educación Grant No. SAB2009-0116.

[1] R. Siebert *et al.*, Nucl. Phys. A **567**, 819 (1994).
[2] A. Gasparian, J. Haidenbauer, C. Hanhart, L. Kondratyuk, and J. Speth, Phys. Lett. B **480**, 273 (2000).
[3] A. Sibirtsev, J. Haidenbauer, H. W. Hammer, and S. Krewald, Eur. Phys. J. A **27**, 269 (2006).
[4] F. Hinterberger and A. Sibirtsev, Eur. Phys. J. A **21**, 313 (2004).
[5] A. Gasparyan, J. Haidenbauer, C. Hanhart, and J. Speth, Phys. Rev. C **69**, 034006 (2004).
[6] A. Gasparyan, J. Haidenbauer, and C. Hanhart, Phys. Rev. C **72**, 034006 (2005).
[7] T. Rozek *et al.*, Phys. Lett. B **643**, 251 (2006).
[8] A. Sibirtsev, J. Haidenbauer, H. W. Hammer, and U. G. Meissner, Eur. Phys. J. A **29**, 363 (2006).
[9] A. Budzanowski *et al.*, Phys. Lett. B **687**, 31 (2010).
[10] B. C. Liu and B. S. Zou, Phys. Rev. Lett. **96**, 042002 (2006).
[11] K. Tsushima, A. Sibirtsev, and A. W. Thomas, Phys. Lett. B **390**, 29 (1997); A. Sibirtsev, K. Tsushima, and A. W. Thomas, *ibid.* **421**, 59 (1998).
[12] R. Shyam, Phys. Rev. C **73**, 035211 (2006).
[13] A. Sibirtsev, J. Haidenbauer, and Ulf-G. Meissner, Phys. Rev. Lett. **98**, 039101 (2007).
[14] S. Abdel-Samad *et al.* (COSY-TOF Collaboration), Phys. Lett. B **632**, 27 (2006).
[15] B. C. Liu and B. S. Zou, Phys. Rev. Lett. **98**, 039102 (2007).
[16] B.-S. Zou and J.-J. Xie, Int. J. Mod. Phys. E **17**, 1753 (2008).
[17] H. X. Yang *et al.* (BES COllaboration), Int. J. Mod. Phys. A **20**, 1985 (2005).
[18] N. Kaiser, P. B. Siegel, and W. Weise, Phys. Lett. B **362**, 23 (1995).
[19] N. Kaiser, T. Waas, and W. Weise, Nucl. Phys. A **612**, 297 (1997).
[20] T. Inoue, E. Oset, and M. J. Vicente Vacas, Phys. Rev. C **65**, 035204 (2002).
[21] J. Nieves, and E. R. Arriola, Phys. Rev. D **64**, 116008 (2001).
[22] C. B. Dover and A. Gal, Prog. Part. Nucl. Phys. **12**, 171 (1985).
[23] P. M. M. Maessen, T. A. Rijken, and J. J. de Swart, Phys. Rev. C **40**, 2226 (1989).
[24] J. Yamagata-Sekihara, J. Nieves, and E. Oset, Phys. Rev. D **83**, 014003 (2011).
[25] J. Gasser and H. Leutwyler, Nucl. Phys. B **250**, 465 (1985).
[26] B. Borasoy, Phys. Rev. D **59**, 054021 (1999).
[27] E. Oset and A. Ramos, Nucl. Phys. A **635**, 99 (1998); E. Oset, A. Ramos, and C. Bennhold, Phys. Lett. B **527**, 99 (2002).
[28] J. A. Oller and Ulf-G. Meissner, Phys. Lett. B **500**, 263 (2001).
[29] G. Alexander *et al.*, Phys. Rev. **173**, 1452 (1968); B. Sechi-Zorn *et al.*, *ibid.* **175**, 1735 (1968).
[30] J. T. Balewski *et al.*, Phys. Lett. B **420**, 211 (1998).
[31] S. Sewerin *et al.*, Phys. Rev. Lett. **83**, 682 (1999).
[32] M. Abdel-Bary *et al.* (COSY-TOF Collaboration), Eur. Phys. J. A **46**, 27 (2010).
[33] J. A. Kadyk, G. Alexander, J. H. Chan, P. Gaposchkin, and G. H. Trilling, Nucl. Phys. B **27**, 13 (1971); J. M. Hauptman, J. A. Kadyk, and G. H. Trilling, *ibid.* **125**, 29 (1977).
[34] F. Hinterberger, S. N. Nedev, and R. Siudak, Int. J. Mod. Phys. A **20**, 291 (2005).